Chemistry and Materials Research
ISSN 2224- 3224 (Print) ISSN 2225- 0956 (Online)
Vol.9 No.9, 2017

A Study of Influence of Anion on Microstructural Development and Sintering of Nanosized Alumina

Fadia Shaheen[1*] Muhammad Irfan[2] Bakht Bahadur Rana[1] Rashad Mahmood[1]
Muhammad Latif Mirza[3]
1.Glass and Ceramic Research Centre, PCSIR Laboratories Complex, Lahore, Pakistan
2.PITMAEM, PCSIR Laboratories Complex, Lahore, Pakistan
3.Department of Chemistry, University of Sargodha, Sargodha, Pakistan

Abstract
Nanosized alumina has been synthesized by employing two aluminum salts with monovalent anions that is aluminum nitrate and aluminum chloride as precursors under identical reaction conditions by homogeneous precipitation method. In both the cases, gelation of aluminum hydroxide occurred in comparable pH regime and produced alumina nanoparticles with comparable average particle size; however their sintering behavior and microstructure of finished products was not comparable. Nanopowders obtained from aluminum nitrate were highly consolidable and sinterable producing reasonable final densities conversely to nanopowders obtained from aluminum chloride which were less consolidable and sinterable, besides the final products showed microstructural flaws including cracks and outgrowths due to inherent passive thermal transformations of nanopowders and unavoidable interferences. DSC/TG, TDA, SEM-EDS, XRD techniques were employed to characterize the nanopowders and dense products.
Keywords: Nanoalumina precursors, aluminum chloride, aluminum nitrate, sintering

Introduction

Nanosized alumina is quintessential ceramic material showing high strength, melting temperature, abrasion resistance, optical transparency and electric resistivity. More recent applications of nanosized alumina include catalyst substrates, tube of Arc lamps, and laser hosts. Possible new uses of nanoalumina are in electronic circuits, optical components, alumina fibers for composite and biomaterials. Traditional uses of alumina are furnace machinery, cutting tools, bearings and gem stones [1]

Ceramic processing to produce ceramic parts with desirable properties is critical to the intrinsic properties of ceramic powders. These include average particle size, particle size distribution, shape, surface area and impurities. Besides method of synthesis of ceramic powders, their fabrication processing also influences the microstructural developments and process of densification.

There are three main routes to synthesize ceramic nanopowders i.e. gaseous, solid and liquid phase. Among these, solution technique is most common and diverse methods to produce nanopowders [2,3]. In the homogeneous precipitation of nanoalumina powders, the influence of anions on the formation of aluminum hydroxide has been investigated by several authors [4-8]. During formation of aluminum hydroxide pH affects critically the crystallinity and morphologies of nanopowder as explained in our previous work [9,10]. It has been reported that monovalent anions NO_3^{1-} and Cl^{1-} both get neutralized in comparable pH regime. It has also been quantified that at precipitation stage, the ratio of added $[OH]^{1-}/[Al]^{3+}$, in both the cases was more than 2.5 at pH value above 5 [4, 11,12]. The present study focuses on the relative effect of monovalent anions primarily on the sol-gel processing and particle profile of nanoalumina powders and subsequently on microstructural developments while densifying into final sintered alumina products..

In the present study alumina nanopowders were produced from aluminum nitrate and aluminum chloride under identical reaction conditions to explore relative effect of monovalent anions

Materials and Methods

Aluminum nitrate nonahydrate $Al(NO_3)_3.9H_2O$ (Fluka) and aluminum chloride hexahydrate $AlCl_3.6H_2O$ (Fluka) were used as starting materials. Molar ratios of aluminum salts and urea $(NH_2)_2CO$ (Merck) are given in Table 1. The sols were heated at 90^{o}C temperature with constant stirring and volume was maintained to 6 liters by adding distilled water. The pH of the sols has been monitored throughout the reaction at definite intervals of time. When pH value reached 7, the reaction was stopped. Gels were washed several times using distilled water. A tray type freeze drier of Max series was used to sublime gels at -40^{o}C. Nanopowders collected from freeze drier were consolidated into green bodies. After presintering at 800^{o}C for 2 hours, the powders were damped with 2wt% (related to Al_2O_3) polyvinyl alcohol PVA (Hoechst, Frankfurt) and uniaxially pressed into 1X0.3" disks. The prerequisites and parameters of cold compaction are given in Table 2.

The green machined compacts were initially dried overnight at room temperature, heated at 100^{o}C for 1 hour in electric oven and finally thermolysed at 800^{o}C for 1 hour. The digital electric laboratory oven WE 500HA and high temperature rapid heating electric furnace RHF/3 Carbolite, UK were used. Sintering was

carried out up to 1400°C at the heating rate 5°C per minute and soaking time 3 hours.

For TDA, specimens with 50 mm length and 20 mm width were fired up to 1600°C @ 20°C per minute in Horizontal Orton Dilatometer DIL 2016 STD.

X-ray diffraction measurements were conducted on Siemen's Diffractometer D5000. X-ray tube operated at 40 kV and 30 mA. Data was collected with a scintillation counter in the 10-70° range with a step of 0.05° and a counting time of 60 s/step.

A Hitachi S-3700, Japan SEM equipped with EDS, was used to acquire image at the accelerating voltage 25 kV, working distance 5 mm, tilt angle 0°. To improve image resolution sample was coated with platinum at 0.1 torr and 20 μA for 2 min which has been found optimum for a thin layer coating.

Result and Discussion

Particle size analysis

Particle profile in Fig 1a reveals that AN3 and AC3 are nanopowders having comparable average particle sizes however; their particle size distribution was different. AN3 has narrower while AC3 has relatively wider particle size distribution. Average particle size of both AN and AC compositions tend to increase as a function of concentration of aluminum salt:urea molar ratio as depicted in Fig 1b.

TDA Studies of AN compositions

Dilatometric curve of AN3 is presented in Fig 2. Up to 800°C, the sample shows shrinkage in three steps; first percent linear change of 0.16% relates to the evolution of adsorbed water, second 0.58% to the dehydroxylation of pseudoboehmite, and third 1.22% to the transformation into gamma alumina with the consequent peaks of shrinkage rate at 100, 231 and 325°C, respectively.

Beyond 800°C, linear shrinkage is 2.14% which depicts that densification begins at 895°C. Almost 80% of this shrinkage is complete up to 1100°C and the remaining 20% up to 1300°C. Two broad peaks associated with this shrinkage region appeared at 1020°C named T_1 and at 1098°C named as T_2. This compound peak shows transformation from θ→α with c.c.p. to h.c.p. structural sequence.

The dilatometric results of AN5, AN7 and AN9 compositions are presented in Fig 3. The general appearance of dilatometric curves of three specimens is same. However, linear shrinkage curves onset at 895, 899, 905, and 911°C, respectively. T_1 and T_2 peaks are ultimately shifted to higher temperatures by few degrees. First peak appeared at 1020, 1024, 1030 and 1036 and second at 1098, 1102, 1109, and 1116°C, respectively. Thus sinterability of AN nanopowders increases with decrease in average particle size and vice versa.

TDA Studies of AC compositions

TDA curve of AC3 in Fig 4 shows that the percentage linear shrinkage due to dehydration is 0.16%, due to dehydroxylation is 0.62% and further due to transformation of pseudoboehmite into gamma alumina is 1.21%. The peaks of shrinkage rate representing these three stages appeared at 100, 300 and 380°C, respectively.

Percentage linear shrinkage from room temperature to 800°C is 1.99% and onwards up to 1400°C is 1.85%. Densification begins at 1052°C with corresponding shrinkage peak at 1107°C.

The densification behavior of rest of three AC compositions is shown in Fig 5. The change in sintering temperature has not been found in uniform with the change in average particle size.

AN and AC compositions showed different densification behavior in various aspects. Firstly, densification in ANs begins about 200 degrees prior to ACs. Secondly, the rate peak is broad and compound in ANs whereas shingle and sharp in ACs. Thirdly, T_1 peak representing θ into α transformation appeared in ANs but not in ACs. Fourthly and finally, percentage linear shrinkage curve in ACs conversely to ANs runs upward after 1200°C showing minor expansion.

SEM studies of AN compositions

AN compositions sintered at 1400°C are presented in Fig 6 a-d. The micrograph image ascertains that sintering is completed. The pores are closed intersecting at the grain boundaries. The grain size is isotropic with almost equiaxial grain shape and average size nearly 1micron. The sintering results show compliance with the dilatometric results.

SEM-EDS studies of AC compositions

AC compositions sintered at 1400°C are shown in Fig 7 a-d. During sintering two modes of damages were identified. One was cracks which appeared throughout the surface. These appeared due to incomplete presintering of AC nanopowders. The green body prepared was defect free while on firing at 1100°C cracks appeared due to incomplete presintering of powders. Fig 8a shows green body and Fig 8b shows cracks after firing 1100°C. AC3 powder presintered at 800°C for 2 hours in Fig 9a shows pseudoboehmite bands along with theta and delta phase. This incompletely dehydroxylated pseudoboehmite produces internal gas pressures while

sintering at elevated temperatures and causes cracks. On the contrary the XRD graph of AN3 in Fig 9b had no traces of pseudoboehmite showing that presintering of powder is complete. Another mode of damage is due to impurities. SEM image and EDS graph are shown in Fig 10a-b. The elements identified are aluminum, oxygen, chloride and traces of iron. Since the impurity emerged out randomly from the plane of sample surface at frequent places so it seems that minor expansion in the dilatometric curve is related to it.

Conclusion

Aluminum nitrate-urea and aluminum chloride-urea were homogeneously precipitated under identical reaction conditions of concentration, dilution, gelating agent, temperature and stirring to produce alumina nanopowders. It was found that both the monovalent anions NO_3^{1-} and Cl^{1-} initiated the gelatinous precipitation at comparable pH, the nanopowders so produced had comparable average particle size, however their relative pre- and post-sintering behavior was incomparable. Alumina nanopowders obtained from aluminum nitrate had higher sinterability as it began at about 200 degrees lower temperature as compared to alumina powders obtained from aluminum chloride under identical fabrication conditions. In the presence of nitrate final densities were reasonable and increase with decrease in particle size whereas in the presence of chloride final densities are neither reliable nor sequential with the change in average particle size as shown in Fig 11. Nanopowders produced from aluminum nitrate sintered to develop isotropic grain size with of 1micron with pores completely closed whereas under identical sintering conditions, nanopowders produced from aluminum chloride exhibited two kinds of flaws. Firstly, cracks due to incomplete dehydroxylation of pseudoboehmite which in turn seems related to particle size distribution. Though average particle size in both the cases was same, however nanopowders from aluminum nitrate had narrow range of particle size distribution as compare to nanopowders from aluminum chloride. Secondly and finally, is the outgrowth of impurities. The source of these two flaws is inherent and thus unavoidable as these appear in early stages and intensify with sintering.

References:

1. Shackelford, J. F., Doremus, R. H., 2008. New Ceramic and Glass Materials. Springer, New York.
2. Matijevic', E. Stryker, L. J., 1966 Coagulation and reversal of charge of lyophobic colloids by hydrolyzed metal ions: III. Aluminum sulfate. J. Coll. Inter. Sci. 22, 68-77
3. Matijevic', E., Janauer, G. E. Kerkers, M., 1964 Reversal of charge of lyphobic colloids by hydrolyzed metal ions. I. Aluminum nitrate. J. Coll. Sci. 19, 333-346.
4. Nagai, H. Hokazono, S. Kato, A., 1991 Synthesis of aluminum hydroxide by a homogeneous precipitation-I Effect of additives on the morphology of aluminum *h*ydroxide Br. Ceram. Trans. 90, 44-48.
5. De Hek, H. Stol, R. J. De Bruyn, P. L., 1978 Hydrolysis-precipitation Studies of aluminum (III) solutions. 3. The role of the sulfate ion. J. Coll. Inter. Sci. 64, 72-89.
6. Stol, R. J. Van, Helden, A. K. De Bryun, P. L., 1976 Hydrolysis-precipitation studies of aluminum (III) solutions. 2 A kinetic study and model. J. Coll. Inter. Sci. 57 115-131.
7. Unuma, H., Kato, S., Ota, T. Takahashi, M., 1998 Homogeneous precipitation of alumina precursors via enzymetic decomposition of urea. Adv. Powder Technol. 9, 181-190.
8. Ramanathan, S., Roy, S. K., Bhat, R., Upadhaya, D. D. Biswas, A. R., 1996 Preparation and characterization of boehmite precursor and sinterable alumina powder from aqueous aluminum chloride-urea reaction. J. Alloy Compd. 243, 39-44.
9. Shaheen, F.; Shah, W. A.; Mirza, M. L. Iqbal, M. P. 2005 Effect of concentration of $Al_2(SO_4)_3$ on the synthesis of Nanosized Alumina. Jour. Chem. Soc. Pak. 27 (6) 602-605
10. Shaheen, F.; Shah, W. A.; Qazi, M. P. I. Mirza, M. L. Development of Nanoparticles of aLumina by sol-gel method using inorganic Aluminum Salts as precursors. Pak. J. Sci. Ind. Res. 49 (2) 77-81, 2005.
11. Vermeulen, A. C. Geus, J. W. Stol, R. J. De Bryun, P. L., 1975 Hydrolysis-precipitation studies of aluminum (III) solutions. I. Titration of acidified aluminum nitrate solutions. J. Coll. Inter. Sci. 51, 449-458.
12. Sato, T. Ikoma, S. Ozawa, F., 1980 Preparation of gelatinous aluminum hydroxide by urea from aqueous solutions containing chloride, nitrate and sulphate of aluminum J. Biotechnol. 30, 225-232.

Table 1: Molar compositions of aluminum salt and urea.

Table 1: Molar compositions of aluminum salt and urea.

Sr. No	Composition Symbol	Salt:Urea molar ratio	Aluminum Salt M/3l	Urea M/3l
1.	AN — AN3, AC3	1:3	0.3	0.9
	AN — AN5, AC5	1:5	0.3	1.5
2.	AC — AN7, AC7	1:7	0.3	2.1
	AC — AN9, AC9	1:9	0.3	2.7

Table 2: Prerequisites and parameters of cold compaction.

Sr. No.	Composition	Pre-sintering Temp/Time (^{o}C/hour)	Binder (2%)	Pressure (MPa)	Time (seconds)
1	AN	800/2	PVA	100	3
2	AC	800/2	PVA	100	3

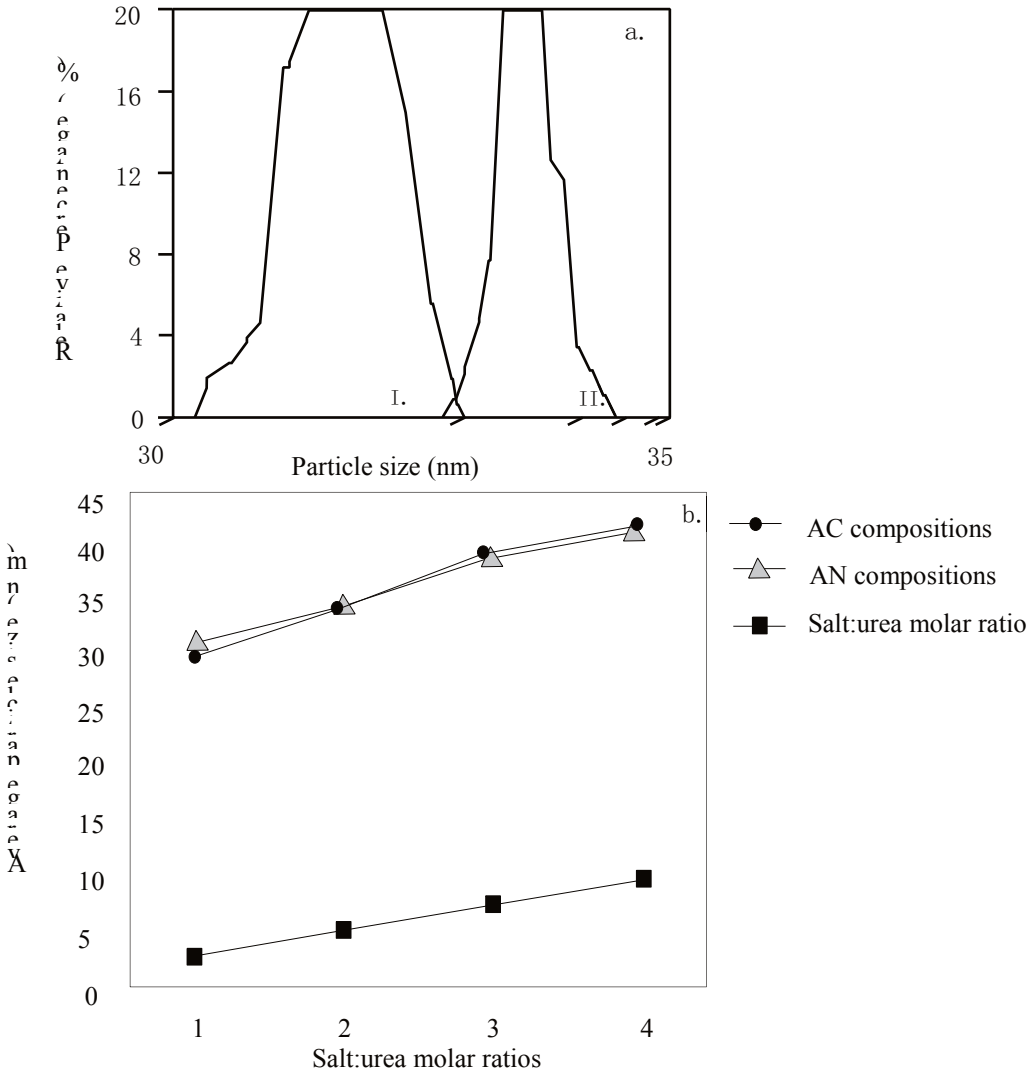

Figure 1: a). Average particle size distribution of I). AN3 and II). AC3 nanopowder and b) Change in average particle size as a function of salt:urea molar ratio.

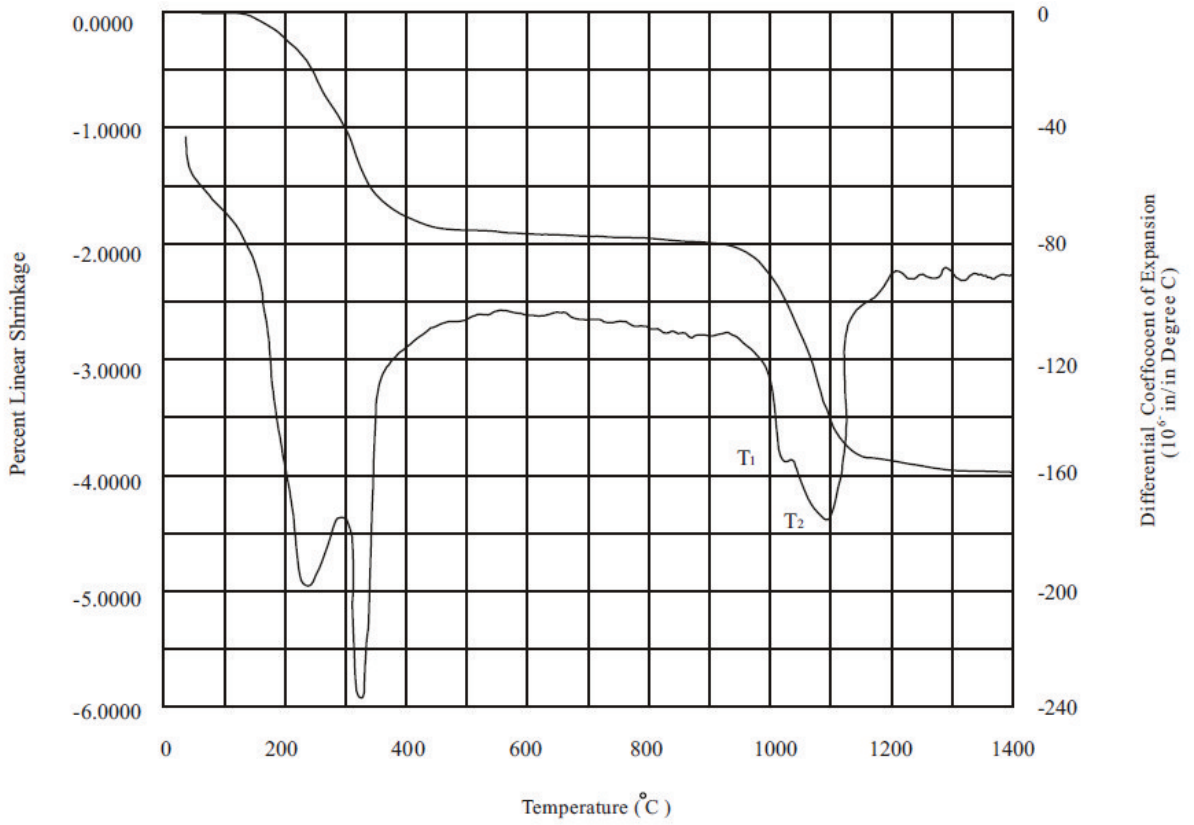

Figure 2: Dilatometric Curve of AN3 composition.

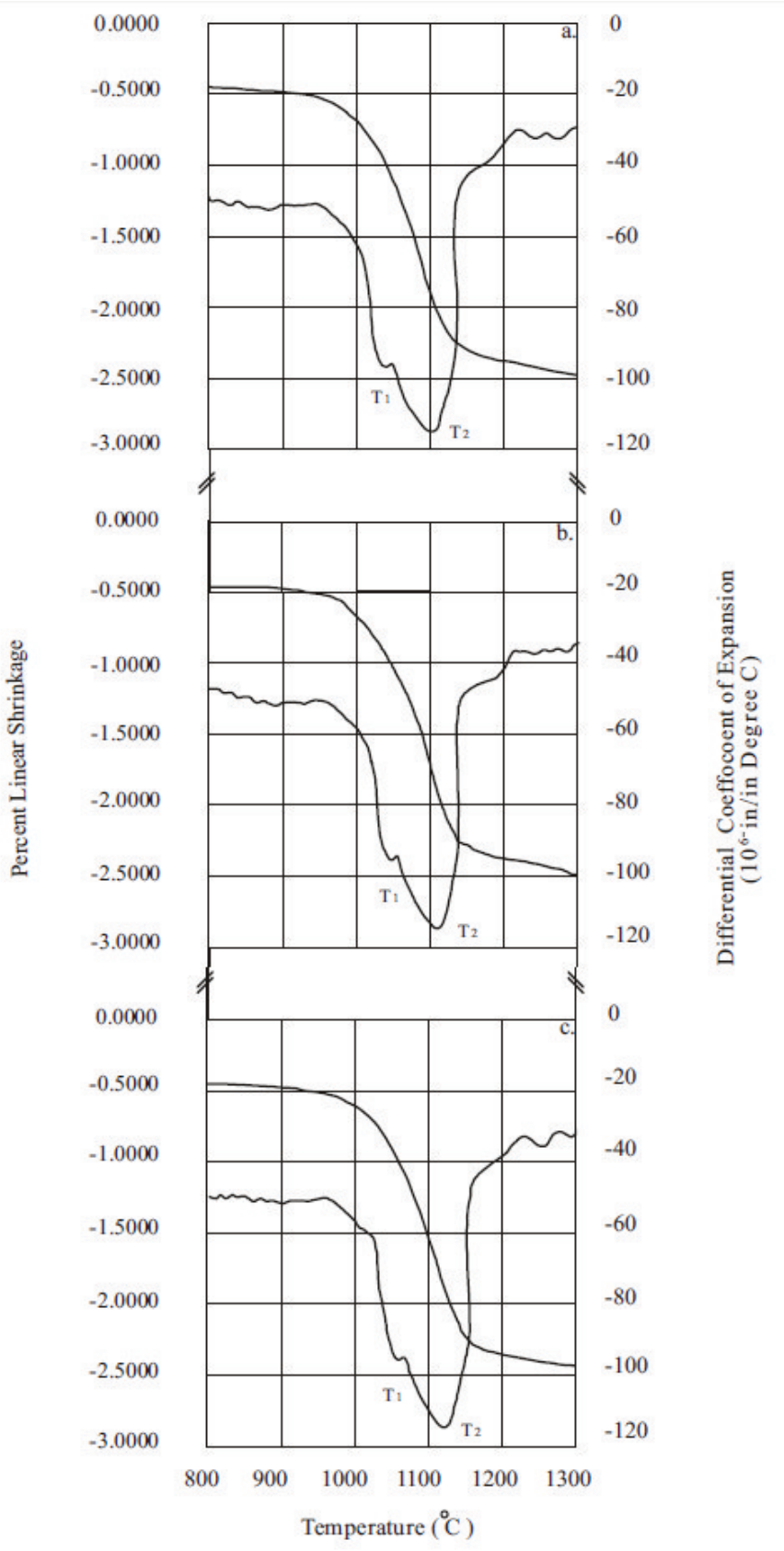

Figure 3: Dilatometric curve of a) AN5, b) AN7 and c) AN9 composition,

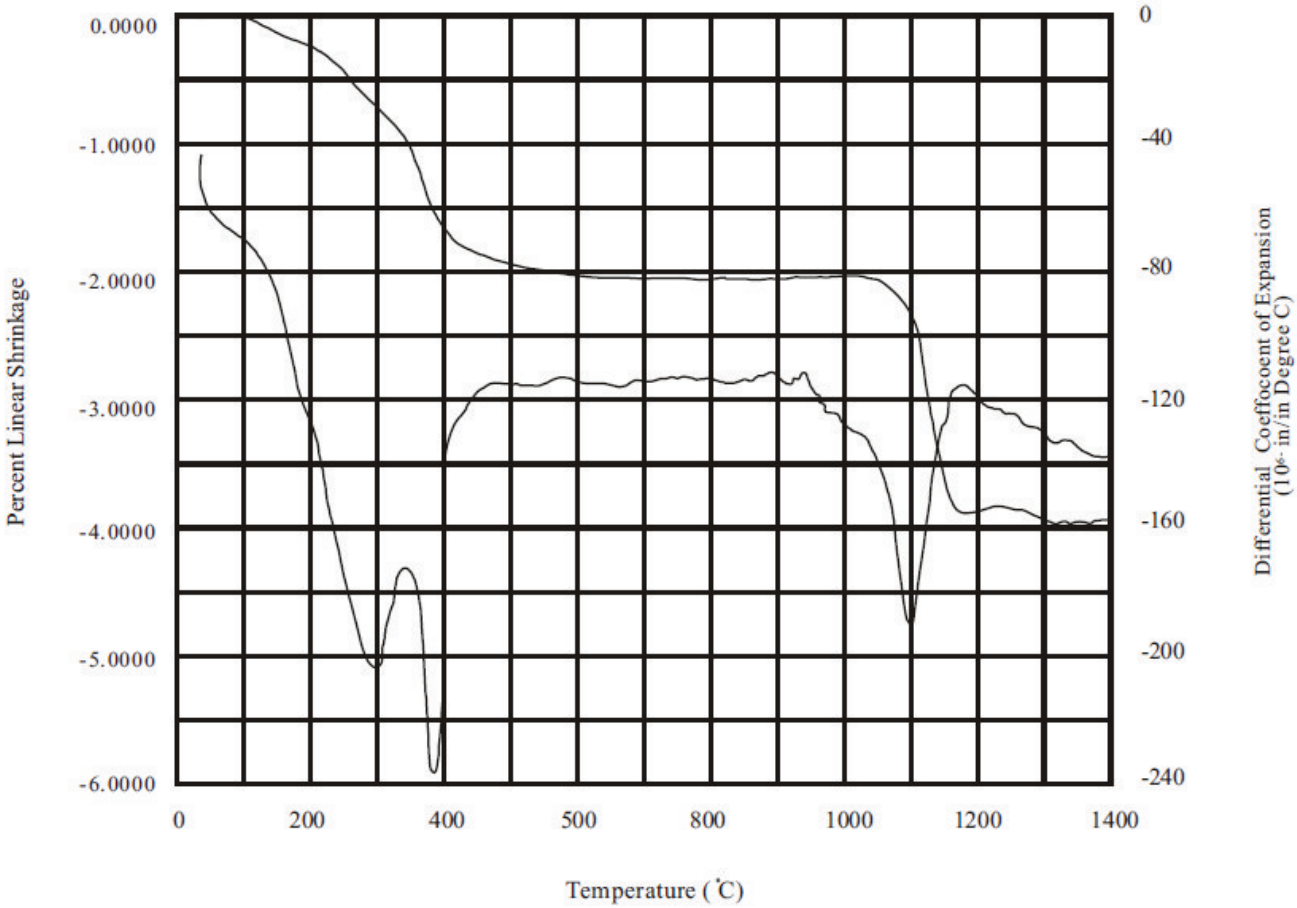

Figure 4: Dilatometric Curve of AC3 composition.

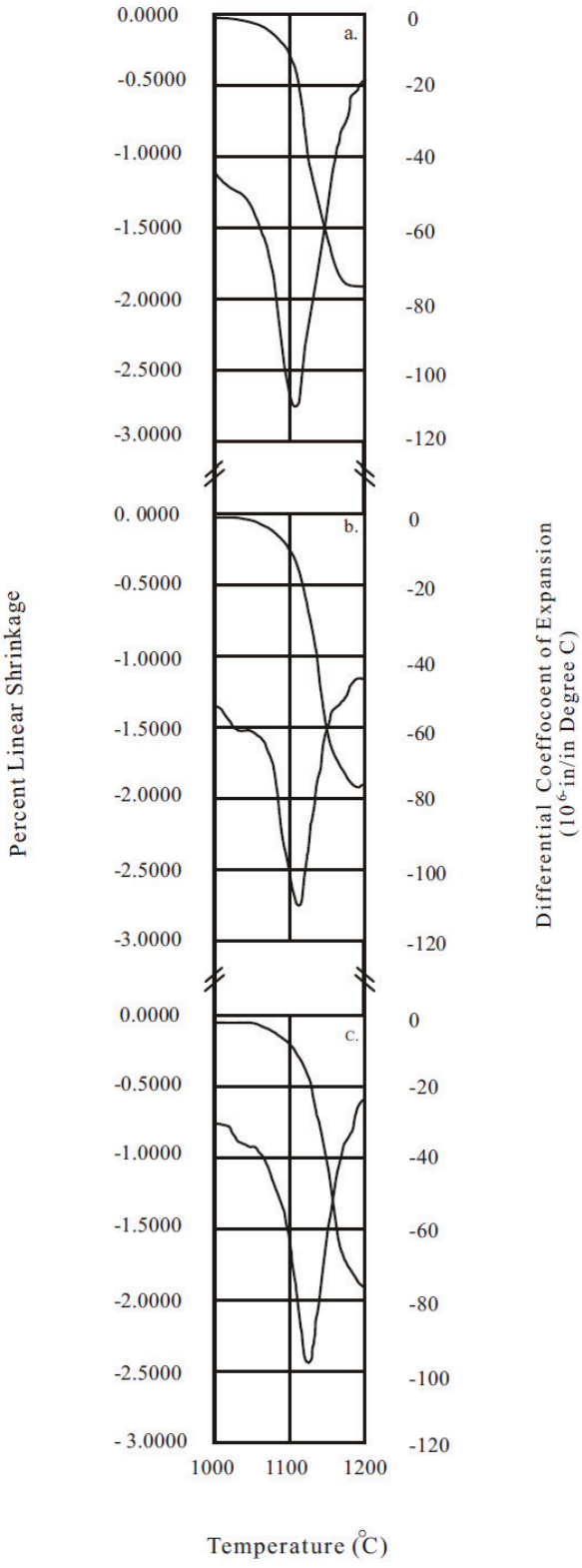

Figure 5: Dilatometric curve of a) AC5, b) AC7 and c) AC9 composition,

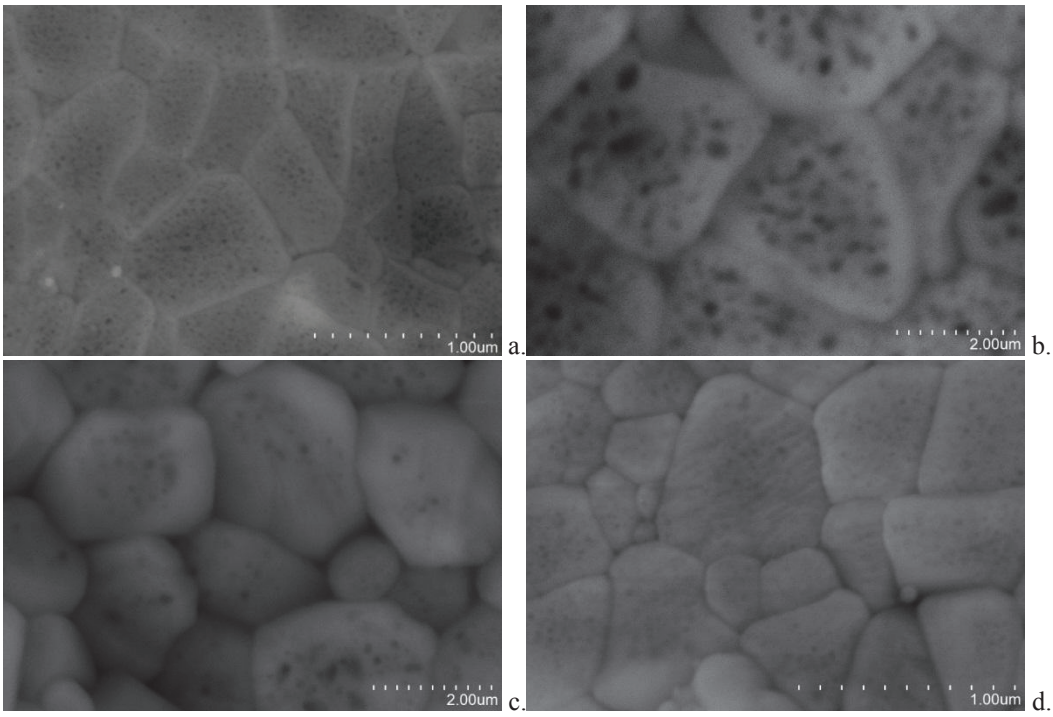

Figure 6: SEM images of a). AN3, b). AN5, c). AN7 and d). AN9 fired at 1400^{o}C

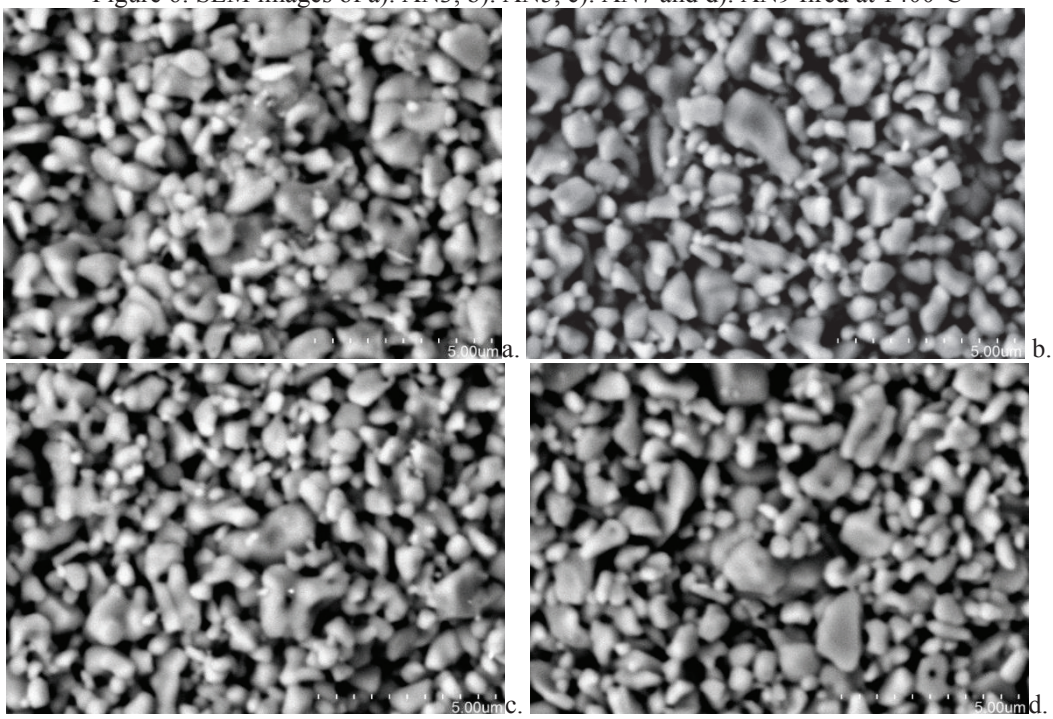

Figure 7: SEM images of a). AC3, b). AC5, c). AC7 and d). AC9 compositions fired at 1400^{o}C.

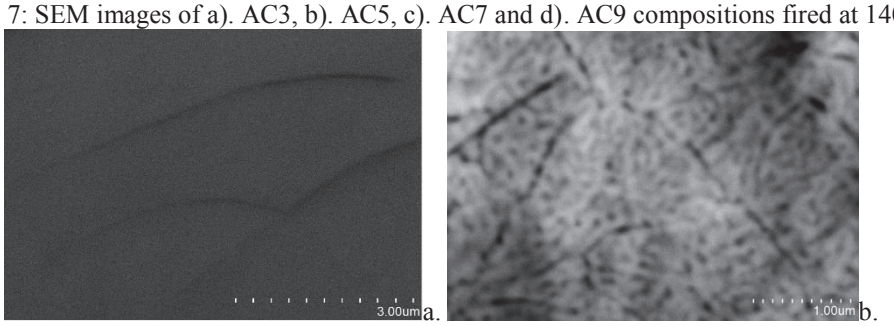

Figure 8: SEM image of AC3 composition a). Green body and b). fired at 1100^{o}C.

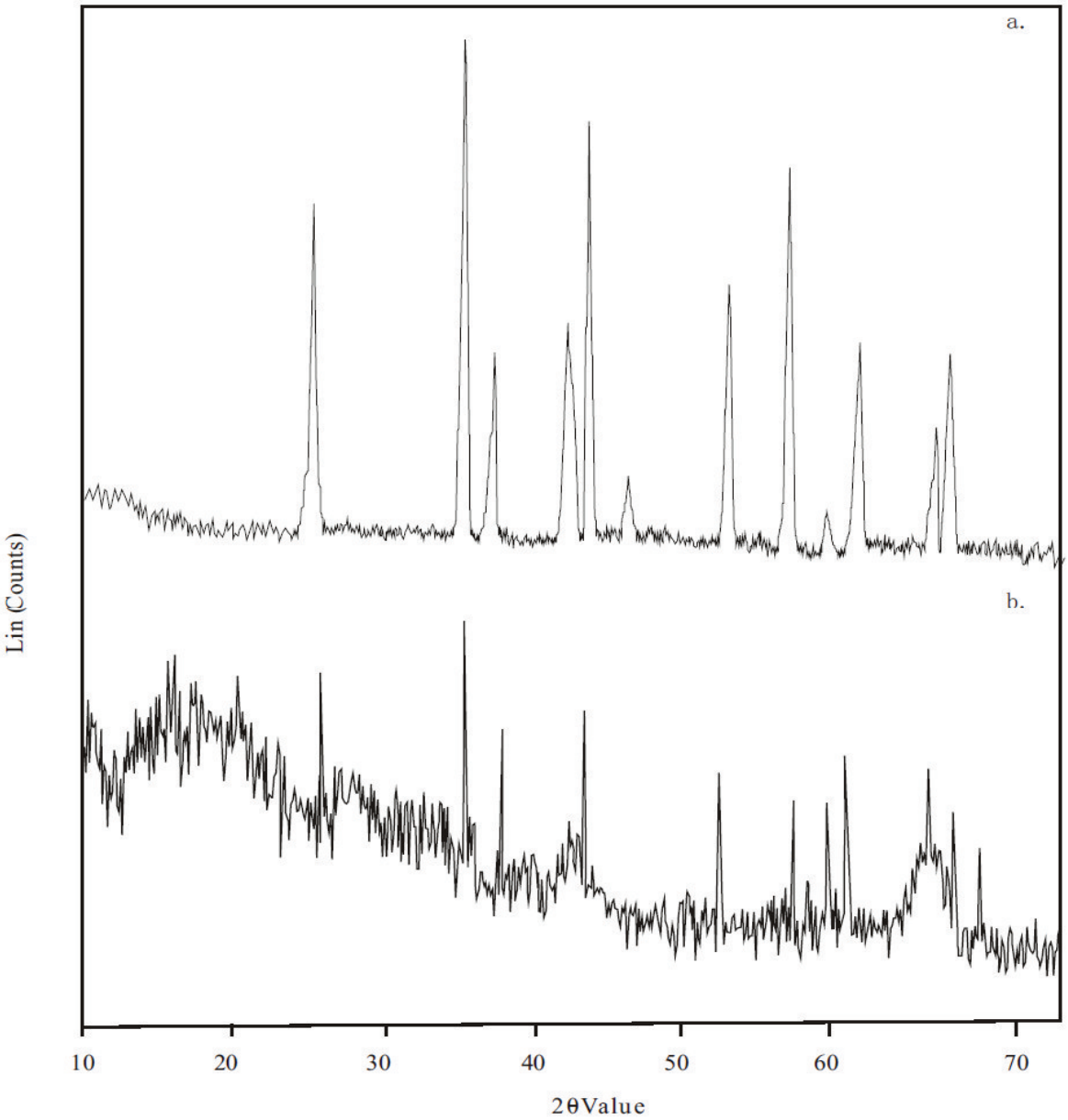

Figure 9: XRD diffractogram of a) AN3 and b) AC3 compositions presintered at 800^{o}C for 2 hours.

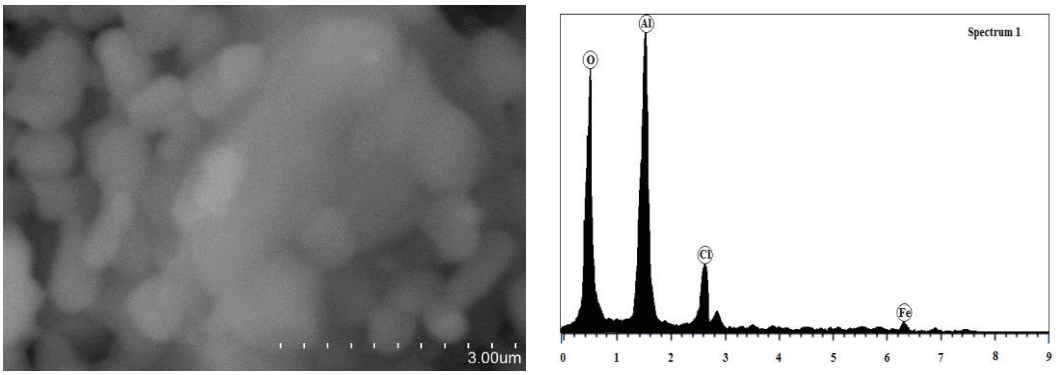

Figure 10: a). SEM image and b). EDS spectrum of Impurity in AC3 composition

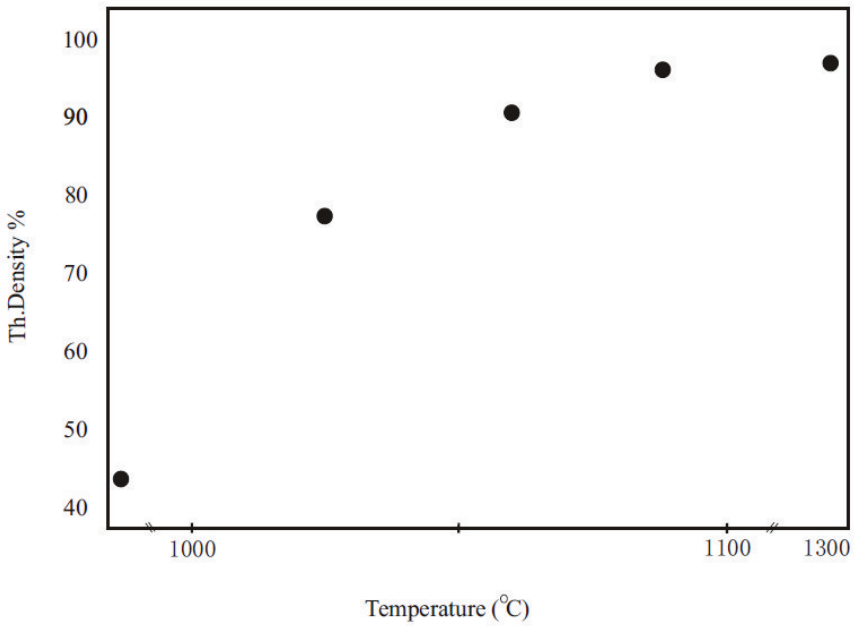

Figure 11: Density variations in AN3 composition with temperature.